Determination of excited-state polarizabilities of Cr^{3+}-doped materials by degenerate four-wave mixing

S. Catherine Weaver
Department of Chemistry, Princeton University, Princeton, New Jersey 08544

Stephen A. Payne
Lawrence Livermore National Laboratory, University of California, P.O. Box 5508, Livermore, California 94550
(Received 4 May 1989)

We have measured the degenerate four-wave-mixing signals from several Cr^{3+}-doped oxide and fluoride laser crystals. The signals are predominantly generated by scattering of the input beams from a refractive index grating that is due to a spatially modulated excited-state population. From the measured reflectivity, the change in polarizability between the ground and excited states of Cr^{3+} is calculated. The polarizability change in the oxide hosts is accounted for by large-oscillator-strength charge-transfer transitions in the energy region of 50 000 cm^{-1}. The fluoride hosts, however, did not give measurable signal levels, and this is attributed to the lack of high-oscillator-strength transitions in this energy range. The polarizability changes in the oxide hosts are observed to depend on the relative thermal population of the $^4T_2$ and the ^2E excited states. The polarizability change between the $^4T_2$ excited state and the $^4A_2$ ground state is found to be greater than that between the ^2E and the $^4A_2$.

I. INTRODUCTION

There is currently a growing interest in the nonlinear properties of impurity ions in ionic solids. In particular, phase-conjugation experiments by four-wave-mixing techniques are used to study these properties. This experiment can be viewed as the creation of a grating in the material by absorption of light by the impurity ions from two interfering laser beams. A third laser beam diffracts off this grating to generate the signal wave. For the case of counterpropagating pump beams, the phase-matching conditions require that the generated signal exactly retraces the path of the probe beam; thus, the signal wave is the phase conjugate of the probe wave. A widely used material for phase conjugation in device applications is $BaTiO_3$. The nonlinearity in $BaTiO_3$ arises from the photorefractive effect, which is due to the local refractive index change arising from charge migration. It is believed that the mobile charge in this material is provided by iron impurities and that the gratings result from the periodic spatial modulation of the 2+ and 3+ valence states of iron.[1] The grating that is generated in a given material may arise from numerous sources other than the photorefractive effect. Other possibilities include gratings of thermal, absorptive, and dispersive origin. Four-wave-mixing (FWM) experiments have been done on gratings that arise from Nd,[2–7] Eu,[8–10] Mn,[11] and Cr-doped[12–26] systems. The main purpose of this paper is to explore the nature of the grating formed in Cr^{3+}-doped ionic systems.

The most extensively studied Cr-doped crystal is ruby, $Al_2O_3:Cr^{3+}$. Early experiments investigated diffraction of light from population gratings in ruby laser rods[27,28] and were interpreted using thick hologram theory.[29] There was some discrepancy as to whether the grating was predominantly absorptive or phase in nature;[13,17,28] however, no conclusive measurements were made. Further experiments included a measurement of the relatively small thermal grating contribution[30] and an upper limit of the diffusion constant for energy transfer was estimated.[31] Ruby was then investigated using degenerate four-wave mixing (DFWM) by Liao and Bloom.[12] They interpreted their results with the theory of Abrams and Lind[32] on DFWM in absorbing media and concluded that dispersion was probably the dominant contribution to the grating. Hamilton *et al.* measured spatial diffusion in ruby and Nd^{3+}-doped glass by DFWM.[13] They interpreted their results in terms of a phase grating and estimated the change in polarizability of the Nd^{3+} and Cr^{3+} ions. Additional FWM experiments in ruby studied the effects of spatial energy migration for different concentrations of chromium,[14] the temporal development of the phase-conjugate signal,[15] and the use of a phase-modulated probe beam wave.[16]

Other Cr^{3+}-doped samples that have been studied in addition to ruby are $BeAl_2O_4$ (alexandrite),[17–19] $YAlO_3$,[20,21] $GdAlO_3$,[22,23] $Gd_3Ga_5O_{12}$ (GGG), $Gd_3Sc_2Ga_3O_{12}$ (GSGG),[24] emerald,[25] and a ceramic with the composition of codierite.[26] Furthermore, the isoelectronic Mn^{4+} ion has been investigated in $Li_4Ge_5O_{12}$.[11] Various aspects of the gratings were studied including energy migration and the temporal properties associated with the Cr^{3+} excited-state population.

We are especially interested in a recent quantitative measurement of the nonlinear refractive coefficient in ruby and $GdAlO_3:Cr^{3+}$ which was obtained using interferometry.[22] With their experimental values for the nonlinear refractive index, Δn, we can calculate the relative

contribution to the scattered signal beam that arises from the different types of gratings (see Sec. II for more details).[33] The relative signals produced by the phase, absorptive, and thermal gratings are approximately $1:10^{-2}:10^{-9}$ for $GdAlO_3:Cr^{3+}$. We see that the absorptive and thermal grating contribution is quite small as suggested by Catunda *et al.*[22] In a separate experiment, they showed that the phase-conjugate signal measured for ruby and $GdAlO_3:Cr^{3+}$ by DFWM agreed reasonably well with the magnitude calculated from their independent measurement of Δn by interferometry.[23] These results are particularly important since they are the first to conclusively show the dispersive origin of phase conjugation in these materials.

In this article we consider whether the phase grating predominates for other chromium-doped systems. In the present work we use the method of DFWM to study a series of Cr^{3+}-doped oxide and fluoride crystals. Our aim is to understand the origin of the change in refractive index of the Cr^{3+} ion that arises with the population of the excited state. We attempt to do this by comparing the four-wave-mixing signals from different host crystals. For example, by comparing the FWM signals of oxides and fluorides, we can determine if the refractive index change arises solely from the electronic structure of Cr^{3+}, or if the nature of the ligand is also of importance. Another comparison of interest is the effect of the strength of the crystal field (CF) the Cr^{3+} ion experiences. Strong CF compounds will have most of the excited-state population in the ^2E state, while weak CF compounds will have more population in the $^4T_2$ state. One objective of our study is to determine if the change in polarizability is different for the ^2E and the $^4T_2$ states relative to the $^4A_2$ ground state of Cr^{3+}.

In this paper, we present theoretical descriptions for the possible mechanisms producing the grating; furthermore, we show that the phase grating contribution is dominant for Cr-doped oxides. We then discuss the origin of the polarizability change in terms of the electronic structure of the impurity host system.

II. THEORY

A. Background

The geometry for DFWM is shown in Fig. 1. This configuration involves the counterpropagating forward and backward pump beams, E_f and E_b, and a weak probe beam E_p. The three incident beams of the same frequency, ω, interact via the nonlinearity of the medium to generate a fourth wave E_s.

A physical interpretation of how the E_s field is produced is shown in Fig. 2. The probe beam interferes with each of the pump beams in the medium, resulting in two gratings having wave vectors of $k_g = k_f - k_p$ and $k_g = k_b - k_p$. Absorption of the modulated light intensity by the Cr^{3+} ions results in a spatial distribution of Cr^{3+} excited states having this same grating pattern. For wavelength λ and angle θ between E_f and E_p, we find that $\Lambda_{fp} = \lambda/[2\sin(\theta/2)]$ is the period of the grating produced by E_f and E_p, and $\Lambda_{bp} = \lambda/[2\cos(\theta/2)]$ is the

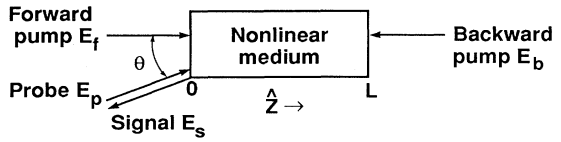

FIG. 1. Degenerate four-wave-mixing (DFWM) geometry. The probe beam E_p propagates at an angle θ, to the counterpropagating forward and backward pump beams, E_f and E_b. Their interaction in the nonlinear medium generates the signal beam E_s. All beams have the same frequency.

period of the grating produced by E_b and E_p. Typically in this arrangement, θ is a small angle and $\Lambda_{fp} \gg \Lambda_{bp}$.

A more complete description of the FWM process considers how the incident electric fields couple through the nonlinear susceptibility of the material to generate the signal wave. In the following, we summarize the results given by Caro and Gower[34] on DFWM in absorbing media. In their terms, we are operating in the low reflectivity regime, all beams are assumed linearly polarized in the same direction, and the pump beams are assumed to be unmodified by the FWM interaction, although their linear absorption is taken into account. The result from their work,[34–36] using the standard methods of the $\chi^{(3)}$ formalism, is expressed as the reflectivity R,

$$R = \left| \frac{E_s(0)}{E_p(0)} \right|^2 \simeq \left| \frac{Q}{a} \right|^2 [1 - \exp(-aL)]^2 \tag{1}$$

where a is the absorption coefficient, L is the sample length, and Q is a factor that depends on the nature of the grating. Here, it has been assumed that we are in the low reflectivity regime, $E_s \ll E_p$, and that $a^2 \gg Q^2$.

From this expression for R we can compare different mechanisms responsible for producing the grating by using the appropriate form of Q, the coupling constant.

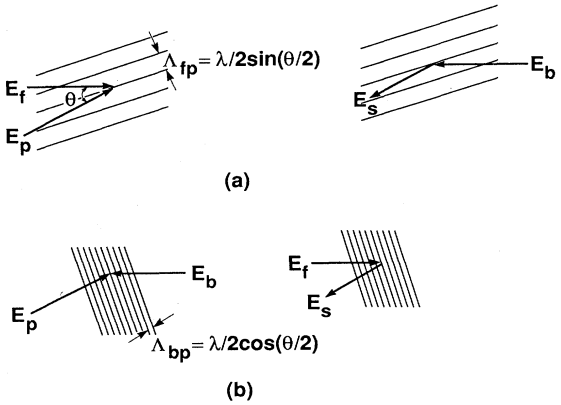

FIG. 2. The two gratings produced by DFWM. In (a) the forward pump E_f and probe E_p beams interfere to produce the large spaced grating, with period $\Lambda_{fp} = \lambda/[2\sin(\theta/2)]$, and similarly in (b) the backward pump E_b and probe produce the small spaced grating, with period $\Lambda_{bp} = \lambda/[2\cos(\theta/2)]$. The phase-conjugate signal beam E_s is generated as the other pump beams are scattered from the gratings.

The types of gratings that are potentially of importance to us include those of absorptive, thermal, and dispersive origin. Below, we discuss the nature of each of the gratings in turn.

B. Absorptive grating

An absorptive grating results from a difference in the absorption cross sections of the ions in their ground and excited states. This type of grating was postulated by Hill[28] to be responsible for the phase-conjugating properties of ruby. Phase conjugation by DFWM in absorbing media was treated by Abrams and Lind.[32] They used the susceptibility expression for a homogeneously broadened two level system in their coupling parameter and obtained an expression for the reflectivity. For the geometry shown in Fig. 1, where $I_f(0)=I_b(L)=I$, the Q can be expressed as[32,34,37]

$$Q_{\rm abs}=\frac{aI}{2I_s}\exp(-aL/2) \tag{2}$$

where I_s is the saturation intensity and is equal to $h\nu/\sigma\tau$, σ is the ground-state cross section, τ is the emission lifetime, and $h\nu$ is the incident photon energy. Note that we take $I \ll I_s$. The experiments give signal power to input power, and we therefore integrate over area assuming Gaussian beam profiles to get the reflectivity for an absorptive grating,

$$R_{\rm abs}=\frac{P_s}{P_p}=\frac{4}{3\pi^2\omega_0^4}\left[\frac{\Delta\sigma\tau}{2h\nu}\right]^2 P_b P_f \times\exp(-aL)[1-\exp(-aL)]^2 . \tag{3}$$

Here P_i is the cw power in the ith beam, and ω_0 is the $1/e^2$ point in the intensity profile of the input beams. We have replaced σ with $\Delta\sigma=\sigma_e-\sigma_g$ to account for the difference in cross section between the ground (g) and excited (e) states. Equation (2) can also be derived on the basis of Kogelnik's hologram theory.[29] The factor of 2 in the denominator arises due to our consideration of only one of the two possible gratings. This assumption is discussed in Sec. IV C.

C. Thermal grating

A thermal grating arises from a change in refractive index due to heating by absorption of energy from the incident fields. This case was treated by Martin and Hellwarth[38] and also by Eichler *et al.*[39] Their results are equivalent if one includes the grating diffusion time in the formulas given by Martin and Hellwarth and the fraction of energy absorbed that is converted to heat Φ in the treatment by Eichler *et al.* The change in refractive index, Δn, is related to the temperature variations by

$$\Delta n=\left[\frac{a\Phi I\Lambda^2}{4\pi^2\kappa}\right]\frac{dn}{dt} , \tag{4}$$

where κ is the thermal conductivity and Λ is the grating spacing. Using the relation between Q and Δn:[34]

$$Q=\frac{\omega\Delta n}{c}\exp(-aL/2) \tag{5}$$

and integrating over the area of the beams gives the reflectivity expected for a thermal grating,

$$R_{\rm th}=\frac{4}{3\pi^2\omega_0^4}\left[\frac{\omega\Phi\Lambda^2}{4\pi^2 c\kappa}\frac{dn}{dT}\right]^2 P_b P_f \times\exp(-aL)[1-\exp(-aL)]^2 . \tag{6}$$

The diffusion time of the grating is given by $t_{\rm th}=\Lambda^2\rho C_p/4\pi^2\kappa$ where ρ is the density and C_p is the specific heat at constant pressure. For the types of crystals we are studying, the diffusion time is calculated to be on the order of a microsecond which is much less than the lifetime of Cr^{3+} in these materials.

D. Phase grating

A (nonthermal) phase grating originates from a difference in the polarizability of the Cr^{3+} ions in their ground state and excited states. A polarizability difference was estimated for ruby and Nd^{3+}-doped glass by Hamilton *et al.* using FWM experiments.[13] More detailed work including the actual measurement of the nonlinear refractive coefficient γ was done by Catunda *et al.*[22,23] on ruby and $GdAlO_3$:Cr^{3+}. The nonlinear refractive coefficient for an optical material is defined by $\Delta n=\gamma I$.[40] The change in polarizability $\Delta\alpha_p$ can be related to Δn starting with the Clausius-Mossotti equation

$$n^2-1=4\pi f_L N\alpha_p , \tag{7}$$

where $f_L=(n^2+2)/3$ is the Lorentz field correction and N is the number density contributing to the polarizability. By taking the derivative of both sides, we see that Δn is proportional to $\Delta\alpha_p=\alpha_e-\alpha_g$, and the excited-state population $N_{\rm ex}$,

$$\Delta n=\frac{2\pi}{n}f_L^2 N_{\rm ex}\Delta\alpha_p . \tag{8}$$

From the rate equations for a three level system and the assumption that $I \ll I_s$, the steady-state fraction of ions in the excited state is given by $Ia\tau/h\nu$. To find the reflectivity in terms of $\Delta\alpha_p$, we use Eq. (5) and integrate over the beam area. This yields the relation for the reflectivity from a phase grating,

$$R_{\rm ph}=\frac{4}{3\pi^2\omega_0^4}\left[\frac{4\pi^2 f_L^2\tau}{cnh}\right]^2\Delta\alpha_p^2 P_f P_b \times\exp(-aL)[1-\exp(-aL)]^2 . \tag{9}$$

As discussed in the Introduction, the relative values for the phase, absorptive, and thermal gratings as described by Eqs. (9), (3), and (6), respectively, are approximately in the ratio of $1:10^{-2}:10^{-9}$ for $GdAlO_3$:Cr^{3+}; see Ref. 33 for a listing of the parameters utilized. We will assume for now that the phase grating is the predominant contributor to the generated signal for the crystals used in the present experiments and then revisit this issue again at the end of Sec. IV.

III. EXPERIMENT

The experimental setup utilized for the DFWM measurements is shown in Fig. 3. A Coherent Radiation model Innova 90-6 argon ion laser was prism tuned to the different lasing lines to provide the pump and probe beams. The four lines used in this experiment were 457.9, 476.5, 488, and 514.5 nm, which excite the low-energy side of the $^4A_2 \rightarrow {}^4T_1(a)$ band of the Cr^{3+} ions in the materials studied. About 5% of the linearly polarized light beam is split off for the probe beam; the remaining light is split into two parts for the pump beams. The total intensity can be continuously varied by a graded neutral-density filter (NDF) at the laser output, and the backward pump-beam intensity can similarly be matched to the forward pump-beam intensity using an additional NDF. The difference in the path lengths of the three beams is less than the coherence length of the laser. The two pump beams are focused into the sample such that they are counterpropagating to each other, and the probe beam enters at about a 2° angle with respect to the forward pump beam. The scattered phase-conjugate signal beam is expected to retrace the path of the probe beam and therefore a beam splitter is used to reflect a portion of this signal to a Si photodiode detector. All beams are chopped to eliminate thermal effects on the signal level. For the transient signal studies, the chopper was replaced with a Vincent Associates Uniblitz shutter so that pulses varying from 2 to 150 ms could be conveniently generated. The detector output is then amplified 100 times prior to being monitored by a boxcar and an oscilloscope, or for the time dependence studies, being fed directly into a transient digitizer. The beam waist and the overlap length were measured using the knife edge technique, giving an ω_0 of about 70 μm (the radius at which the intensity profile drops to $1/e^2$ of its peak value). Taking the internal angle of the beams in the samples into account, we calculated that all three beams are overlapped for more than 5 mm. Since our longest samples were of this order, no path length corrections are required. The beam power was monitored with a photodiode-scatter plate assembly that was carefully calibrated with a thermopile. Typical pump beam energies were 1 mJ in chopped pulses of 2.5 ms; the probe beam energy was approximately 15% of the pump-beam energy.

The signals from different crystals are compared by measuring them relative to a single sample; we choose GSGG:Cr^{3+} as our standard crystal in these experiments. This way any variation in the laser intensities or the alignment are likely to be cancelled. In comparing relative signals, however, one must take the surface reflectivity R into account by dividing the measured result by $(1-R)^4$. From Eq. (9) we see that an absorption correction of $\exp(-aL)[1-\exp(-aL)]^2$ must be included to appropriately compare crystals having different Cr concentrations and cross sections. The optical densities for each crystal were obtained from absorption spectra taken on a computer controlled Cary-17 spectrophotometer. The FWM experiments required that the crystals be polished to high quality to reduce the scattered light background, and to minimize the realignment for different samples. A system of shutters was used to determine the residual scattered light level by blocking one or more of the three input beams. Each set of measurements was made several times and alternated with a measurement of the standard crystal. The reproducibility of the relative signals measured this way was within 20%. The absolute reflectivity was measured for GSGG:Cr^{3+} in a separate experiment. To obtain the polarizability change, quantitative measurements including the beam power, beam waist, sample absorption, and the emission lifetime were made. Finally, the optical system itself was calibrated by replacing the GSGG:Cr^{3+} sample with a mirror to determine the absolute reflectivity arising from the phase-conjugation process.

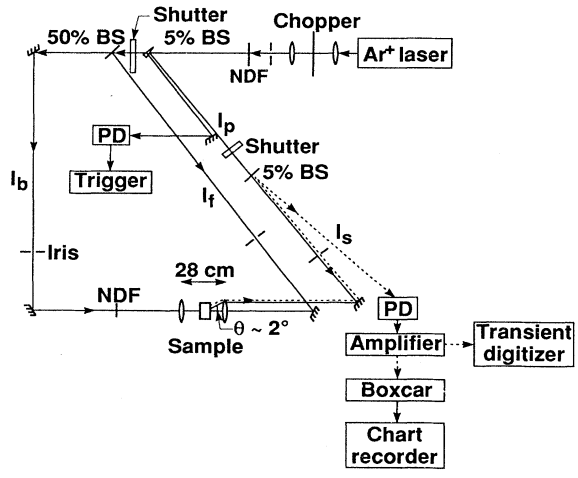

FIG. 3. Experimental setup used for the DFWM measurements. NDF, graded neutral-density filter; PD, photodiode; BS, beam splitter.

IV. RESULTS

A. Background of the Cr^{3+} ion

The visible absorption spectrum of octahedrally coordinated Cr^{3+} is due to d-d transitions between crystal-field states. The room-temperature absorption spectrum of Cr^{3+}-doped $Gd_3Sc_2Ga_3O_{12}$ is shown in Fig. 4. The general features shown in this spectrum are representative of nearly all Cr^{3+}-doped materials. The bands centered at about 640 and 460 nm are the vibronically broadened spin-allowed $^4A_2 \rightarrow {}^4T_2$, and $^4T_1(a)$ transitions, respectively. These states have a different electronic configuration than the ground state and are associated with the $t_2^3 \rightarrow t_2^2 e$ transition. For the case where the $^4T_2$ is the lowest state, a broad emission band arising from the $^4T_2 \rightarrow {}^4A_2$ transition is observed in the near infrared. Characteristic lifetimes of the $^4T_2$ state vary from 10 to 300 μs depending on the host crystal. The $^4A_2 \rightarrow {}^2E$ and $^2T_1$ transitions are seen as negative features superimposed on the $^4T_2$ band around 690 and 670 nm, respectively. These are spin-forbidden transitions and have the

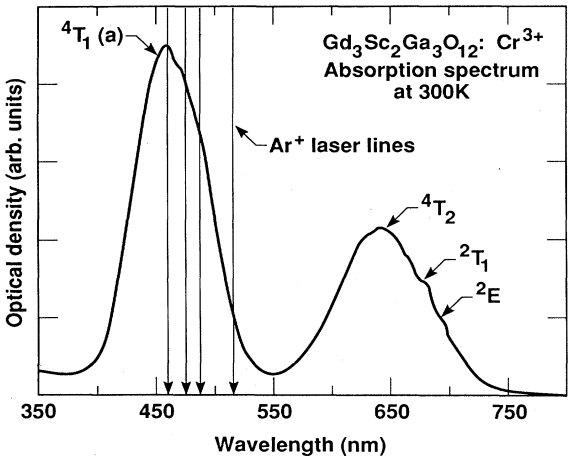

FIG. 4. Absorption spectrum of $Gd_3Sc_2Ga_3O_{12}$:Cr^{3+}. The Ar^+ laser lines used in this experiment are indicated. The actual peak optical density of the $^4T_1(a)$ band is 0.94, and the sample length is 0.178 cm. The main features observed in this spectrum are representative of most Cr^{3+}-doped materials.

same t_2^3 electronic configuration as the ground state. For some systems, the host interactions are much stronger and as a result, the $^4T_2$ state is shifted to higher energy, and the ^2E becomes the lowest excited state. Here a sharp line is observed in the emission spectrum and is characterized by an emission lifetime that is in the rage of 1–50 ms. In crystals where the $^4T_2$ and the ^2E state are both thermally populated, the lifetime of Cr^{3+} is, of course, intermediate between the values for either state.

The argon laser lines used for the FWM experiments are indicated on the absorption spectrum. Their positions relative to the absorption spectrum are similar for all the materials studied; that is, they are on the low-energy side of the $^4T_1(a)$ peak. For the fluoride host, this band is shifted to slightly higher energy so that only the 476.5- and 457.9-nm lines have substantial absorption. While the absorption between the two bands falls to nearly zero for many materials, the hosts with multiple sites tend to have a higher level of absorption in this region. For example, $BeAl_2O_4$ and $LaMgAl_{11}O_{19}$ (LMA) have more than one octahedral site and the absorption between the two major bands is probably from Cr^{3+} ions in these different sites. In $BeAl_2O_4$:Cr^{3+} (alexandrite) there are two distinct sites known as the mirror site and the inversion site. Approximately 75% of the Cr^{3+} ions occupy the mirror sites, while the remaining Cr^{3+} ions occupy the inversion site and have been shown to absorb in the region between the major absorption bands of the mirror sites.[41–43] As it turns out, the mirror sites exhibit stronger oscillator strength and therefore dominate most of the observed optical properties. The inversion site is characterized solely by ^2E emission and has a lifetime of nearly 50 ms, in contrast to the 240-μs lifetime of the mirror site, which exhibits mixed $^4T_2$ and ^2E emission properties. In the LMA host, there are three octahedrally coordinated aluminum sites where the Cr^{3+} may substitute. The lifetimes of these sites have been measured as 0.28, 1.0, and 2.7 ms.[44] All of the other materials studied in this work have a single type of octahedral site available for Cr^{3+} substitution. In the next section, we will demonstrate the validity of the phase-conjugate reflectivity expression derived earlier, Eq. (9), by experimentally verifying that the Cr^{3+} ions in GSGG form a phase grating which is due to the polarizability difference between the ground and excited states.

B. Experimental validation of theory

We previously showed with an order of magnitude calculation of $GdAlO_3$:Cr^{3+} that the observed FWM signal is likely to be from a grating of dispersive origin. We also derived a detailed expression for the FWM signal in terms of the change in polarizability of the Cr^{3+} ions:

$$P_s = \frac{4}{3\pi^2\omega_0^4}\left[\frac{4\pi^2 f_L^2 \tau}{cnh}\right]^2 \Delta\alpha_p^2 P_f P_b P_p \times \exp(-aL)[1-\exp(-aL)]^2 , \quad (9')$$

where P_s/P_p has been substituted for $R_{\rm ph}$. All the variables in this equation are measurable except for $\Delta\alpha_p$, the difference in polarizability between the ground and excited states of Cr^{3+}. In this section, we demonstrate the validity of this expression by showing the intensity, lifetime, and wavelength dependences of the FWM signals.

To begin with, the intensity dependence was measured by translating a graded neutral-density filter at the laser output. In this manner, the total laser power could be smoothly varied, and the signal variation was measured against the total input power. A log-log plot of the FWM signal versus the input intensity in GSGG:Cr^{3+} is shown in Fig. 5. The measured data have a best fit slope of 2.7

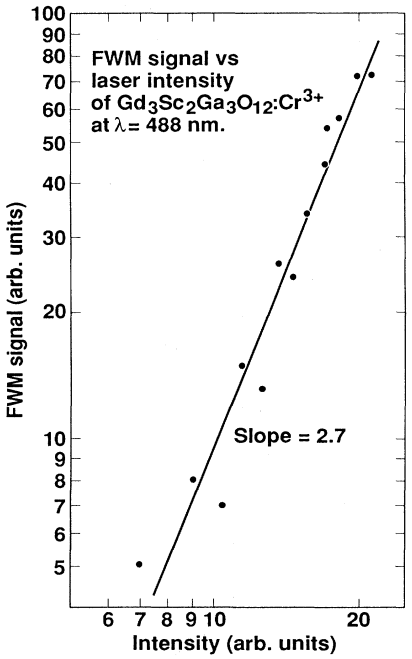

FIG. 5. Measured DFWM signal of $Gd_3Sc_2Ga_3O_{12}$:Cr^{3+}, at λ=488 nm, plotted on a logarithmic scale as a function of the total incident laser intensity. The best fit slope of 2.7 is in agreement with the I^3 dependence predicted by Eq. (9').

which is close to the cubic dependence predicted by Eq. (9'). Although the intensity scale is labeled as arbitrary, it is proportional to W/cm^2. This result verifies that, for the pump and probe intensities used in these experiments, the undepleted beam approximation used in deriving Eq. (9') is valid. Additionally, we confirmed that the FWM signal disappeared when any of the three input beams was blocked. Any residual scattered light arising solely from the pump or probe beams was subtracted from the total signal. Similar measurements obtained for the alexandrite sample gave a best fit slope of 2.8.

The temporal response of the FWM signals was studied by varying the lifetime of the Cr^{3+} ions in GSGG. For all the crystals where the lifetime of Cr^{3+} is much less than the laser pulsewidth, the excited-state population is in a steady-state regime. Thus in order to study the time dependence of the FWM signal in these crystals, we varied the lifetime by changing the crystal temperature. For the case of GSGG:Cr^{3+}, we found that by increasing the crystal temperature the Cr^{3+} lifetime steadily decreases from 115 μs at room temperature to 77 μs at 400 K. This change was significant enough that the FWM signal lifetime dependence was readily observable. A log-log plot of the signal versus the lifetime in GSGG:Cr^{3+} is shown in Fig. 6. The optical transmission of this crystal at 488 nm was also measured as the temperature was raised. Since the transmission was observed to decrease slightly with rising temperature, an absorption correction was necessary to isolate the effect of the Cr^{3+} lifetime. Thus the signals were corrected for absorption using the expression, $\exp(-aL)[1-\exp(-aL)]^2$ as derived in Eq. (9'). With the absorption taken into account, the time dependence data gives a best fit slope of 1.9 which is close to the τ^2 dependence expected from the form of Eq. (9').

In Fig. 7 the time dependences at 488 nm for all the oxide crystals studied are shown. For the hosts GSGG ($\tau=115$ μs), $Gd_3Sc_2Al_3O_{12}$ (GSAG, $\tau=150$ μs), Ga_2O_3 ($\tau=185$ μs), and $ScBO_3$ ($\tau=115$ μs), the FWM signal was constant as the laser pulses were varied from 0.3 to 5.2 ms as they are in the steady-state regime. These results are plotted in Fig. 7(a). For crystals with lifetimes comparable to or longer than the laser pulsewidth, the time dependence was studied by determining the functional form of the rise time of the FWM signal. A simple rate equation approach for a three level system[45] shows

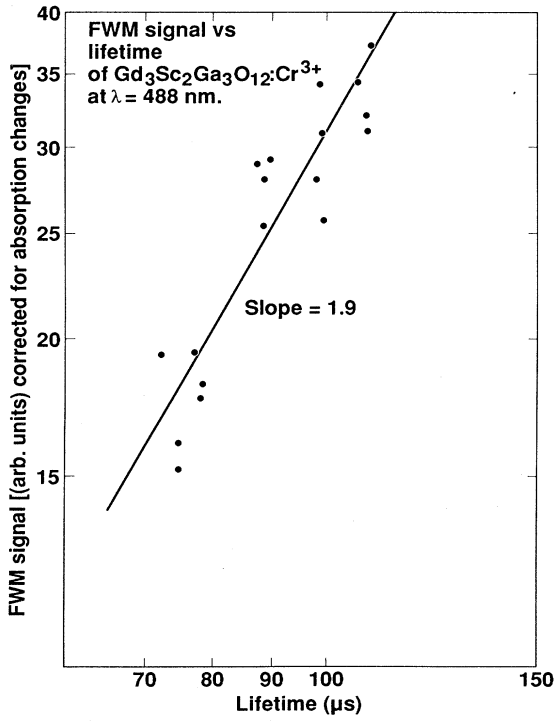

FIG. 6. Measured DFWM signal of $Gd_3Sc_2Ga_3O_{12}:Cr^{3+}$, at $\lambda=488$ nm, plotted on a logarithmic scale as a function of the emission lifetime. The lifetimes were varied by increasing the crystal temperature from 300 to 400 K; the FWM signals were also corrected for absorption changes at the different temperatures. The best fit slope of 1.9 is in agreement with the τ^2 dependence predicted in Eq. (9).

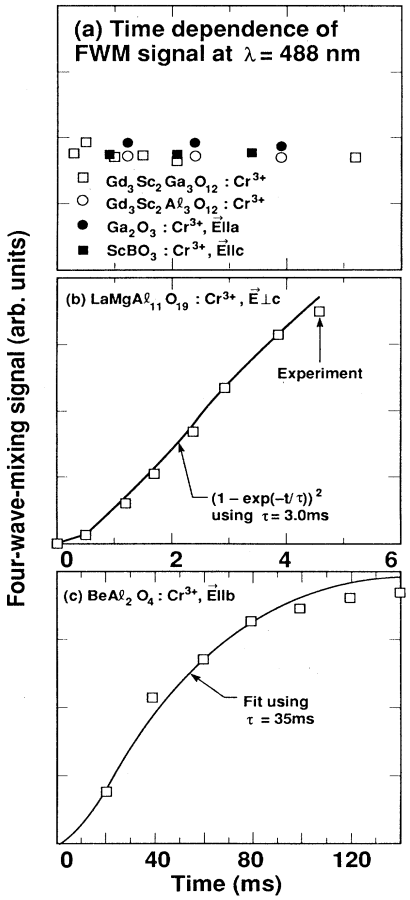

FIG. 7. Time dependence of the FWM signals for all the oxide crystals at $\lambda=488$ nm. (a) For crystals with emission lifetimes short compared to the laser pulsewidth, a steady-state regime is reached and the signal is constant with time. For $LaMgAl_{11}O_{19}:Cr^{3+}$ (b) and $BeAl_2O_4:Cr^{3+}$ (c), the Cr^{3+} lifetime is longer than the laser pulsewidths and therefore the FWM signal rises as $[1-\exp(-t/\tau)]^2$.

that the excited-state population N_{ex} should rise as $1-\exp(-t/\tau)$, where t is time and τ is the emission lifetime. The FWM signal is dependent on N_{ex}^2 and therefore the signal should be proportional to the expression $[1-\exp(-t/\tau)]^2$. For the other two crystals shown in Fig. 7, alexandrite and LMA:Cr^{3+}, the signal follows this dependence when the laser pulsewidths are similar to the Cr^{3+} lifetime. The FWM signal in LMA:Cr^{3+} versus time is shown in Fig. 7(b). The data (points) were fit to the above time dependence (solid line) with a best fit giving $\tau=3.0$ ms. This is in accordance with the emission lifetime measurements of the different sites in LMA:Cr^{3+}. The 3.0-ms time constant also suggests that the site with the longest lifetime is the dominant contributor to the FWM signal. Similarly, excitation at 488 nm in alexandrite leads to an excited-state population mainly in the inversion sites. The temporal response of this system was studied using pulsewidths of up to 150 ms. The FWM signal in alexandrite as a function of time is shown in Fig. 7(c). Again, the data were fit to the above time dependence using $\tau=35$ ms. This time constant is close to previous measurements of the inversion site lifetime of 44 ms suggesting this site gives the dominant contribution to the FWM signal at 488 nm. We also note here that the lowest possible laser intensities were used to avoid saturating the signal, as was observed in Ref. 19. In summary, the results reported in Figs. 6 and 7 show that the time dependence of the FWM signal is given by $\tau^2[1-\exp(-t/\tau)]^2$ and that when t/τ is large this expression reduces to a simple τ^2 dependence.

A final aspect of the FWM process characterizing the Cr^{3+} impurities is illustrated through the wavelength dependence. In Fig. 8 the FWM signal of GSGG:Cr^{3+} at four different wavelengths is displayed. In these measurements, the total laser intensity was kept constant for each of the wavelengths, and additionally the signal was corrected for the $I_f I_b I_p$ product since its value changed slightly due to the wavelength dependence of the beam splitters. The FWM signals were corrected for absorption and also for the changing Si detector response at different wavelengths. As indicated in Fig. 8, the corrected FWM signal is constant for different excitation energies within experimental error. The significance of this result is found by considering the pumped difference absorption spectrum.[46] Using the experimental apparatus described in Ref. 47, the difference in the absorption cross section between the ground and excited states of GSGG:Cr^{3+} has been obtained and is reproduced in Fig. 8. The change in absorption cross section goes through a maximum and a minimum within the wavelength range used for the FWM measurements. If the grating were of absorptive origin, the FWM wavelength dependence should be strongly correlated with the difference spectrum. Since it is not, this confirms our earlier calculations that an absorptive grating is unlikely to play an important role in generating the FWM signal. In fact, the data in Fig. 8 provide evidence that the grating is of dispersive origin. Since the FWM signal is constant over the wavelength range studied, however, we must conclude that the polarizability difference between the ground and excited states is not influenced by the d-d transition depicted in the lower frame of Fig. 8, but that it must result from higher lying, although stronger transitions. This point will be addressed in greater detail in Sec. V.

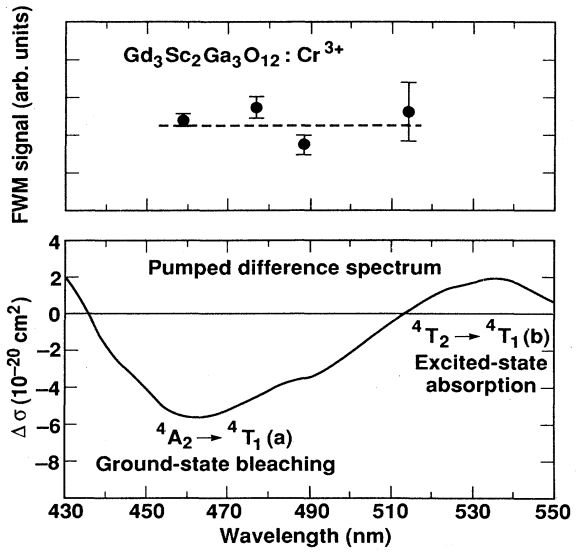

FIG. 8. Upper frame: Wavelength dependence of $Gd_3Sc_2Ga_3O_{12}:Cr^{3+}$ FWM signal. Signals were corrected for laser intensity, absorption, and detector response at each wavelength, and within experimental error, they are constant. Lower frame: Pumped difference absorption spectrum. This spectrum was obtained by pumping the Cr^{3+} ions to the excited state, and then interrogating the change in absorption that results; the positive signal is excited-state absorption, the negative signal is ground-state bleaching. Since this spectrum does not correlate with the FWM spectrum, we conclude that an absorptive grating is not important.

The wavelength dependence of alexandrite also shows an interesting effect. Now, since the absorption features of alexandrite primarily arise from the mirror site, we would expect the FWM excitation spectrum to have a constant value (as it did for GSGG), only if the mirror sites also gave rise to the FWM signal. This is not the case, however, as is seen from Fig. 9. As mentioned earlier, the laser lines in this experiment excite in between the main absorption bands in alexandrite and are probably absorbed primarily by mirror site ions, although the FWM signal from the inversion sites is nevertheless likely to dominate, since its lifetime is much longer (44 versus 0.24 ms). This was demonstrated by the long time dependence of 35 ms at 488 nm as shown in Fig. 7(c). A further confirmation of the importance of the inversion site is shown in Fig. 9 where the emission excitation spectrum of the inversion site is compared with the wavelength dependence of the FWM signal (corrected for absorption and laser intensity). The correlation of these two spectra is important because it shows that even though the ground-state absorption for mirror site ions is larger, the long lifetime of the inversion site ions results in the greater contribution to the FWM signal. In other words,

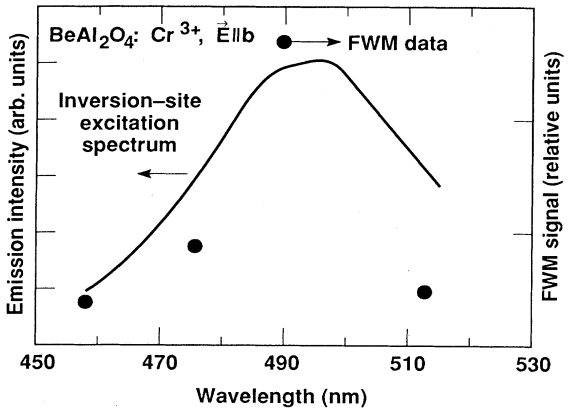

FIG. 9. Wavelength dependence of $BeAl_2O_4:Cr^{3+}$ FWM signal plotted with inversion site excitation spectrum (Ref. 42) for comparison. The FWM signal was corrected for absorption and laser intensity. The correlation of these two spectra indicates that the inversion site ion is the dominant contributor to the FWM signal at the wavelengths used in this experiment, while the gross features of the absorption spectrum are due to the mirror site Cr^{3+} ions.

the FWM experiment has extracted out the absorption due to the inversion site, in spite of the fact that the mirror sites are essentially responsible for the properties of the absorption spectrum. This contrasts with the case of GSGG:Cr^{3+}, where there is only one kind of Cr^{3+} site.

C. Determination of polarizability change $\Delta\alpha_p$

As mentioned earlier, the FWM signals of the different crystals are best compared by measuring them relative to a single sample. The standard crystal chosen for this purpose was GSGG:Cr^{3+}. All the crystals studied are listed in Table I. The thickness, the linear refractive index,[48–54] the emission lifetime of Cr^{3+},[42,45,47,55–57] and the optical density at the four Ar^+ laser wavelengths used are tabulated for each crystal. Relative values of the FWM signal for each sample were obtained by taking the average of several measurements of that crystal and dividing it by the average of several measurements of GSGG:Cr^{3+}. To minimize the effect of any long-term experimental fluctuations, the measurements of the standard and unknown were made in an alternating sequence. The relative signals are then corrected for surface reflections, absorption, and emission lifetime. The corrected signal $\beta_{\rm rel}$ is then given by

$$\beta_{\rm rel}=\frac{P_u}{P_s}\frac{(1-R_s)^4}{(1-R_u)^4}\frac{\exp(-aL)_s[1-\exp(-aL)_s]^2}{\exp(-aL)_u[1-\exp(-aL)_u]^2}\times\frac{\tau_s^2[1-\exp(-t/\tau_s)]^2}{\tau_u^2[1-\exp(-t/\tau_u)]^2}\ , \tag{10}$$

where P_u is the unknown signal and P_s is the standard signal. The corrected FWM signals $\beta_{\rm rel}$ for each crystal are reported in Table I for the wavelengths where the optical density is between about 0.1 and 0.6, since this is the range where the absorption correction is likely to work well. The signals that are listed were reproducible within about 20%; omissions in the table indicate that those signals were either not observed or not consistent. In the case of $La_3Ga_5SiO_{14}:Cr^{3+}$ (LGS), there was no signal observed, presumably because the emission lifetime is only 6 μs. We mention at this point that the absence of signal in LGS:Cr^{3+} provides further evidence that there is not a thermal grating contribution involved, since for a thermal grating only the fraction of energy converted to heat is important and the emission lifetime has no bearing on the grating efficiency. Additionally, the FWM signals from all the fluoride crystals were less than the noise level and therefore must be less than 5% of the GSGG:Cr^{3+} signal. Using the relative value of 0.05 in Eq. (10), an upper limit for the corrected signal in the fluorides is listed.

The change in polarizability can be calculated from the measured reflectivity using Eq. (9). Solving Eq. (9) for $\Delta\alpha_p$ gives the expression for the change in polarizability:

$$\Delta\alpha_p(cgs)=\left[\frac{3R_{\rm ph}}{4}\right]^{1/2}\frac{cnh\omega_0^2}{4\pi f_L^2\tau P_f}\times\frac{1}{\exp(-aL/2)[1-\exp(-aL)]}\ . \tag{11}$$

The absolute reflectivity measured for GSGG:Cr^{3+} was 3.0×10^{-3}. The other values used in Eq. (11) for this calculation are $\omega_0=70$ μm, $\tau=115$ μs, the absorption correction, $\exp(-aL/2)[1-\exp(-aL)]$, at 488 nm is 0.373, and $P_f=P_b=0.38$ W. The $\Delta\alpha_p$ calculated from these values is 0.114 Å^3. We note that one of the two possible gratings shown in Fig. 2 generates most of the signal. This was confirmed to be the case through polarization dependence studies used to isolate the individual contributions from the two gratings. For the case of GSGG:Cr^{3+}, we found that the contribution from the small spaced grating dominated by about 8:1, over the large spaced grating. Therefore, when calculating the polarizability, we assumed the measured reflectivity was from predominantly one grating.

Using the reflectivity measured for GSGG:Cr^{3+}, the absolute reflectivity for the other samples was obtained from their relative values given in Table I. The polarizability difference was then calculated for each crystal using the data obtained from Eqs. (10) and (11) and is shown in Table II. The average value of the reflectivity at all the wavelengths measured was used in the polarizability calculation for all crystals except alexandrite for which the reflectivity at 488 nm was used since this wavelength corresponds to the peak of the inversion site absorption spectrum (see Fig. 9). Again, an upper limit is given for the fluoride crystals since their signals were below our detection limit. Also listed in Table II for comparison is the energy separation ΔE between the ^2E and the $^4T_2$ levels. For the crystals where the $^4T_2$ level is below the ^2E level, ΔE is taken from the low-temperature absorption spectrum as the energy distance between the $^4T_2$ origin and the negative feature superimposed on the $^4T_2$ band from the ^2E absorption.[47,58–61] When the ^2E is below the

TABLE I. Relative DFWM signals, β_{rel}, and sample properties [see Eq. (10)], at indicated Ar laser wavelengths.

Crystal:Cr^{3+}		Thickness (mm)	Linear refractive index	Lifetime (μs)	Optical density/λ (nm) 457.9	476.5	488	514.5	Corr. signals, β_{rel}/λ (nm) 457.9	476.5	488	514.5	References
$Gd_3Sc_2Ga_3O_{12}$		1.78	1.99	115	0.90	0.84	0.62	0.19	1	1	1	1	47,48
$Gd_3Sc_2Al_3O_{12}$		5.46	1.89	150	1.06	0.80	0.55	0.11			0.254		47,49
$ScBO_3$	$E\perp\hat{c}$	4.66	1.87	115	0.59	0.51	0.32	0.10	0.286	0.282	0.284		47,50
	$E\parallel\hat{c}$		1.82		0.46	0.38	0.22	0.07	0.077	0.141	0.175		
$BeAl_2O_4$	$E\parallel\hat{b}$	3.27	1.76	44 000[a]	0.34	0.14	0.06	0.17	0.0014	0.0028	0.010	0.0018	42,47,51
	$E\parallel\hat{a}$		1.75		0.55	0.16	0.10	0.12	0.0012	0.0022	0.0052	0.0020	
Ga_2O_3	$E\parallel\hat{a}$	1.54	1.96	185	>2.00	1.70	1.10	0.24				0.306	52,57
	$E\perp\hat{a}$				1.50	1.44	1.06	0.26				0.341	
$LaMgAl_{11}O_{19}$	$E\perp\hat{c}$	2.05	1.80	300–3000	0.46	0.30	0.25	0.36	0.035	0.032	0.030	0.031	44,53
	$E\parallel\hat{c}$		1.79		0.44	0.33	0.20	0.23	0.012	0.018	0.033	0.027	
$La_3Ga_5SiO_{14}$	$E\perp\hat{c}$	2.35	1.76	6	0.64	0.31	0.30	0.05	b				54,55
	$E\parallel\hat{c}$				0.12	0.14	0.26	0.05					
$Na_3Ga_2Li_3F_{12}$		3.40	1.37	310	0.36	0.18	0.04	0.01	<0.003	<0.002			47
$SrAlF_5$	$E\parallel\hat{a}$	2.00	1.4	95	0.54	0.40	0.23	0.02	<0.038	<0.010			47
	$E\parallel\hat{c}$				0.55	0.24	0.16	0.02	<0.038				
$LiCaAlF_6$	$E\parallel\hat{a}$	5.55	1.39	175	0.18	0.07	0.03	0.00	<0.019				56
	$E\parallel\hat{c}$				0.12	0.04	0.02	0.00	<0.033				

[a] Inversion site.

[b] No signal was observed in $La_3Ga_5SiO_{14}$ due to the short lifetime of Cr^{3+}.

TABLE II. Polarizability change calculated from DFWM signals.

Crystal:Cr^{3+}		$\alpha_{ex}-\alpha_g$ (Å^3)	ΔE_{0-0} (cm^{-1}) ($^4T_2-^2E$)	References
$Gd_3Sc_2Ga_3O_{12}$		0.114[a]	+50	62
$Gd_3Sc_2Al_3O_{12}$		0.062	+285	49
$ScBO_3$	E⊥ĉ	0.067	−1300	58
	E∥ĉ	0.047		
$BeAl_2O_4$	E∥b̂	0.015	+5500[b]	41,63
	E∥â	0.010		
Ga_2O_3	E∥â	0.065	+560	64
	E⊥â	0.068		
$LaMgAl_{11}O_{19}$	E⊥ĉ	0.024	+1100	59
	E∥ĉ	0.020		
$Na_3Ga_2Li_3F_{12}$		<0.01	−1400	47
$SrAlF_5$	E∥â	<0.04	−1900	60
	E∥ĉ	<0.04		
$LiCaAlF_6$	E∥â	<0.02	−700	61
	E∥ĉ	<0.03		

[a] Measured value.
[b] Inversion site.

$^4T_2$ but close enough in energy that the $^4T_2$ is thermally populated, the energy separation is found by fitting the temperature dependence of the lifetime to an equation describing emission from two levels.[41,49,62–64] This energy separation is of interest here because it indicates the fraction of the excited-state population that is in each state. In Table II, we see that $\Delta\alpha_p$ is in the range of 0.05–0.11 Å^3 for oxides with the $^4T_2$ state largely populated, but for the crystals where the excited-state population resides predominantly in the ^2E state, the $\Delta\alpha_p$ has a tendency to be smaller, with values of 0.01–0.07 Å^3. Furthermore, in the fluoride crystals, where the $^4T_2$ is the lowest excited state, the change in polarizability is markedly lower than in the oxides with similar energy level ordering. The origin of these trends is complicated, but plausible mechanisms will be discussed further in the next section.

At this point, it is appropriate to revisit the question of the relative magnitude of the absorptive and phase gratings. The relative signal levels can be calculated by dividing Eq. (9) by (3), giving

$$\frac{R_{ph}}{R_{abs}}=\left[\frac{8\pi^2 f_L^2 \bar{\nu}\Delta\alpha_p}{n\Delta\sigma}\right]^2. \tag{12}$$

We calculate this ratio using the upper limit for R_{ph}, obtained with the $\Delta\alpha_p$ from Table II (this value was found assuming a pure phase grating), and the upper limit for R_{abs} obtained using the maximum value of $\Delta\sigma$ for the resonant d-d transition depicted in the lower frame of Fig. 8. We thus find that $R_{ph}/R_{abs}=37$ for GSGG:Cr^{3+}, indicating that the absorptive grating makes a negligible contribution in this particular case. Unfortunately, the $\Delta\sigma$ values are unavailable for the other samples studied in this work. However, if we calculate the maximum value for R_{abs} (that occurs when $\Delta\sigma$ is equal to the ground-state absorption cross section), then R_{ph}/R_{abs} is close to unity for LMA:Cr^{3+}. It is therefore possible that the absorption grating may make a non-negligible contribution to the materials with the lowest $\Delta\alpha_p$ values, including LMA:Cr^{3+} and alexandrite. Given the unavailability of the $\Delta\sigma$ values, we can only regard the $\Delta\alpha_p$ values of LMA and alexandrite as being estimates at this time. We can also assume that the signals generated from the materials giving the larger $\Delta\alpha_p$ values (GSGG, GSAG, $ScBO_3$, and Ga_2O_3) are predominantly due to the phase grating contribution.

Several uncertainties remain in regard to the data in Table I. For example, it appears that the β_{rel} values of $ScBO_3$:Cr^{3+} show a wavelength dependence for the E∥ĉ spectrum, although the E⊥ĉ polarization is roughly constant, as expected. Similarly, only one polarization shows the expected constant β_{rel} values for LMA:Cr^{3+} as well. The reason for these observations is unknown at this time, and may be due to the existence of multiple sites or to experimental error.

It is important to remark that our main conclusions are not affected by the aforementioned complications, since we have successfully measured the $\Delta\alpha_p$ values of several materials without interference from the absorptive grating contribution. In addition, the main conclusion regarding LMA:Cr^{3+} and alexandrite is that their $\Delta\alpha_p$ values are much smaller than those of the other crystals.

V. DISCUSSION

In the previous sections, we provided evidence that the FWM signals observed in Cr^{3+}-doped crystals are generated predominantly from a phase grating which is due to a spatially modulated excited-state population. The experimental results confirmed the theoretical predictions of the intensity and lifetime dependences of the FWM signals, and the change in polarizability between the ground and excited states of Cr^{3+} was calculated from the measured phase-conjugate reflectivity. This interpretation shows that the excited state has a different refractive index than the ground state, and the experimental

evidence indicates that this difference is dependent on the local environment of the Cr^{3+} ions. We now discuss in more detail the origin of this refractive index change in terms of the electronic structure of the Cr^{3+}-host system.

The typical oscillator strengths of d-d transitions in Cr^{3+}-doped systems are on the order of 10^{-4}–10^{-5}. However, charge-transfer (CT) transitions have been observed in Cr^{3+}-doped oxides[46,65,66] around 50 000 cm^{-1} having oscillator strengths in the range of 0.1 to 0.01. In particular, Andrews *et al.*[46] have observed an intense uv charge-transfer band in the excited-state absorption spectra of GSGG and GSAG:Cr^{3+}. In the GSGG host, the CT band peaks at about 48 000 cm^{-1} relative to the ground state and has a width of $\Delta\bar{\nu}=6700$ cm^{-1} and an oscillator strength of 0.03. The contribution to the polarizability from a single CT state of cross section σ_{CT} and at energy $\bar{\nu}_{CT}$ in units of cm^{-1} is calculated with[67]

$$\alpha_{CT}=\frac{1}{4\pi^3}\frac{9n}{(n^2+2)^2}\frac{1}{\bar{\nu}_{CT}^2-\bar{\nu}^2}\int\sigma_{CT}(\bar{\nu})d\bar{\nu}\ . \tag{13}$$

For incident radiation at 488 nm, we calculate the polarizability difference, $\Delta\alpha_p=\alpha_e^{CT}-\alpha_g^{CT}$ using the above data from Andrews *et al.* and find $\Delta\alpha_p=0.20$ Å^3. This value is in reasonable agreement with our experimental result of 0.114 Å^3 obtained for GSGG:Cr^{3+} indicating that the CT band is probably the dominant contributor to the polarizability change observed.

The idea that the high-oscillator-strength charge-transfer transitions are the origin of the polarizability change observed in Cr^{3+}-doped oxides may also explain why the polarizability changes in fluoride systems were found to be small (see Table II). The energy of a CT transition is determined in part by the ionization potential of the ligand. Therefore, for an oxide host, the ligand to metal CT state is at a lower energy than in a fluoride host. Accordingly, CT transitions have not been observed in Cr^{3+}-doped fluorides in this energy region, but instead, the $3d\rightarrow 4s$ intraionic transitions have been observed, as reported by Sabatini *et al.*[68] From their data on a series of divalent transition metal ions in $KMgF_3$, CaF_2, and MgF_2, we estimate the typical oscillator strength for a $3d\rightarrow 4s$ transition to be about 2×10^{-3} with a peak frequency near 56 000 cm^{-1} and width of $\Delta\bar{\nu}=4000$ cm^{-1}. Using this information, we calculate a typical change in polarizability in a fluoride host to be 0.007 Å^3 with Eq. (13). Thus the $d\rightarrow s$ transitions in fluorides give a polarizability change that is an order of magnitude smaller than that found in oxides due to the CT contribution.

In Fig. 10 an energy level diagram showing the relationship of the charge-transfer band to the change in polarizability between the excited state and the ground state is illustrated. The pump beams excite the Cr^{3+} ions, in a spatially periodic pattern, into the $^4T_1(a)$ band from which they rapidly relax into the lowest excited state, either the $^4T_2$ or the ^2E. The scattering efficiency of the probe beam then depends on the difference $\alpha_e-\alpha_g$. This change, as we showed in Eq. (13), depends on the strength of the contributing transition and the energy separation from the states being probed. Thus for

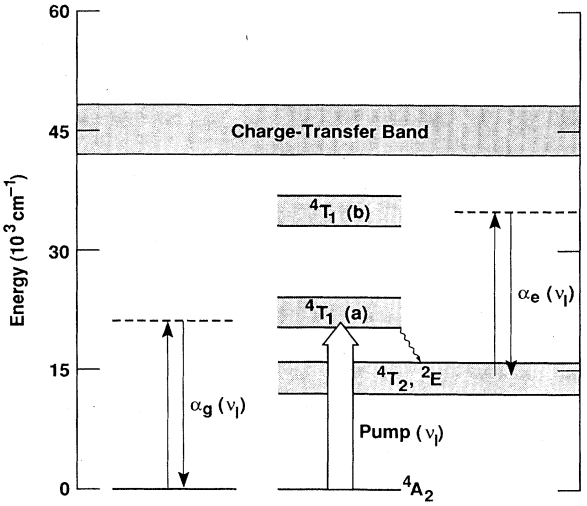

FIG. 10. Energy level diagram showing the Cr^{3+} energy levels and the ligand-to-metal charge-transfer band relevant in the DFWM experiments for oxide host crystals. The FWM experiment probes the difference in polarizability from the ground state and lowest excited state, and the magnitude of this difference depends on the strength and energy separation of the charge-transfer band, see Eq. (13).

fluoride systems, we can consider the same interaction, only the CT band is replaced with a much weaker $3d\rightarrow 4s$ intraionic band. The $\Delta\alpha_p$ is then much smaller and the scattered signal is expected to be accordingly less, as observed.

In the preceding paragraphs, we have discussed how Cr^{3+}-doped oxide compounds are more polarizable than Cr^{3+}-doped fluoride compounds. We would now like to relate these ideas to the classical concepts of polarizabilities. According to Tessman, Kahn, and Shockley,[69] the electronic polarizability of O^{2-} in ionic crystals is proportional to the volume it occupies. The volume that the O^{2-} ion occupies in Ga_2O_3 and Cr_2O_3 is similar, and thus by comparing their molecular polarizabilities and assuming the O^{2-} contribution remains constant, we can estimate the polarizability of Cr^{3+} in Cr_2O_3. Using the refractive index of 2.551 for Cr_2O_3 (Ref. 70) and 1.962 for Ga_2O_3 (Ref. 52) and the free ion polarizability for Ga^{3+} of 0.20 Å^3,[71] we find the polarizability of O^{2-} to be 1.92 Å^3 and that of Cr^{3+} to be 0.86 Å^3. The calculated Cr^{3+} polarizability of 0.86 Å^3 does not represent solely the metal ion, but also the high degree of covalent interaction between Cr^{3+} and O^{2-} as well. Since, in the FWM experiment, we are measuring a change in polarizability of the entire Cr^{3+}-O^{2-} moeity we can estimate that the percent polarizability change is $0.114/0.86=13\%$. This seems reasonable since the $^4T_2$ excited state probably has a different bonding interaction with the oxygens than does the $^4A_2$ ground state.

As discussed in Sec. III, the polarizability differences given in Table II indicate that there is a tendency for the ^2E level of Cr^{3+} to have a smaller $\Delta\alpha_p$ than the $^4T_2$ level. To analyze this in further detail, we assume that the total polarizability is the sum of a contribution from the ^2E

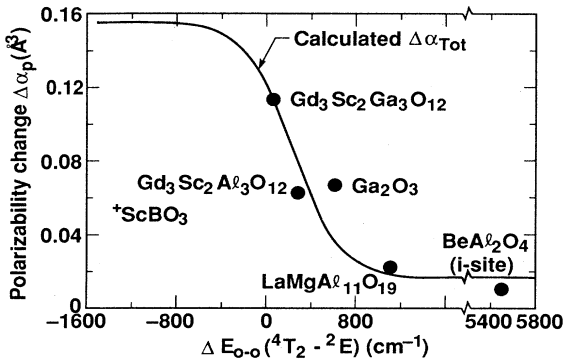

FIG. 11. The measured polarizability change plotted as a function of the $^4T_2$-^2E energy separation. The total polarizability change is a sum of contributions from the $^4T_2$ and the ^2E states α_T and α_E, weighted by the Boltzmann factor of their relative populations at room temperature. The solid line is the polarizability change calculated from $\alpha_T=0.155$ Å^3 and $\alpha_E=0.017$ Å^3, see Eq. (14). $ScBO_3$ does not fit in with these data because the nature of the oxygen ligand is modified by bonding with boron.

and the $^4T_2$ levels weighted by a Boltzmann factor of their relative populations. In LMA:Cr^{3+} and alexandrite, the energy separation is such that the sole contribution to the polarizability observed is from the ^2E level. Taking the average value of $\Delta\alpha_p$ from these crystals, 0.017 Å^3, as the ^2E polarizability, α_E, we can find the $^4T_2$ polarizability, α_T, with this expression:

$$\Delta\alpha_{\text{tot}}=f_T\alpha_T+f_E\alpha_E \ , \tag{14}$$

where $\Delta\alpha_{\text{tot}}$ is the measured change in polarizability, and f_T and f_E are the Boltzmann factors for the $^4T_2$ and ^2E levels, respectively, and are given by

$$f_i=\frac{g_i \exp(-\Delta E/kT)}{\sum_i g_i \exp(-\Delta E/kT)} \ , \tag{15}$$

where $i=E$ or T corresponds to the ^2E and $^4T_2$ states. The degeneracy g is 12 for the $^4T_2$ state and 4 for the ^2E state. This gives an α_T of 0.155 Å^3. Using Eqs. (14) and (15) to calculate $\Delta\alpha_{\text{tot}}$ for a range of ΔE values, the measured polarizability changes can be fit to this curve with the ΔE values of the crystals used in this work from Table II. The polarizability change measured for each crystal is plotted against the $^4T_2-{}^2E$ energy separation in Fig. 11 and the calculated $\Delta\alpha_{\text{tot}}$ curve is plotted for comparison. The main assumption is that a single set of α_E and α_T values can be used to adequately represent a large range of crystals. The measured data are close to the calculated values, with the exception of $ScBO_3$:Cr^{3+}, confirming that this model is appropriate for most of the crystals. The anomalous result for $ScBO_3$:Cr^{3+} is explainable, however, since in this crystal, the oxygen ion is no longer describable as O^{2-} but instead is intimately bound to the boron atom, forming a $(BO_3)^{3-}$ molecular anion of trigonal symmetry.

Finally, we consider the origin of the difference in the polarizability between the ^2E and the $^4T_2$ states. The fact that the polarizabilities are different is not surprising since the excited-state geometry for the $^4T_2$ is different from the $^4A_2$ ground state while for the ^2E it is the same. As a result of the many effects operating simultaneously, a quantitative comparison between the two states is difficult to formulate. The nature of the charge-transfer bands must also play a role here, in addition to the geometry changes. For example, as the crystal field increases, the $^4T_2$ level is raised to higher energies and the excited-state population will reside mainly in the ^2E level leading to a smaller observed polarizability. The stronger crystal field may indicate, however, that the O^{2-} ion is more ionic, and perhaps, that the charge-transfer bands are shifted to higher energy. Furthermore, since the ^2E and $^4T_2$ states have different spin values, they are expected to have strong CT transitions only to those CT states having the same spin.[72] This effect will also give rise to a difference in the polarizability of the $^4T_2$ and ^2E states. The effects of the excited-state geometry, spin selection rules, and the CT bands are interrelated and individual contributions of each would be problematic to separate out. The main conclusion at this time is simply that the $^4T_2$ state exhibits a larger polarizability change relative to the $^4A_2$ than does the ^2E state.

VI. CONCLUSION

We have studied the DFWM signals from several Cr^{3+}-doped oxide and fluoride crystals in order to determine the nature of the grating formed. Theoretical formalisms were presented to describe gratings of thermal, absorptive, and phase origin. An order of magnitude calculation using these formulas indicated that absorptive and thermal contributions would generally be smaller. Indeed, since the thermal diffusion time is much smaller than the Cr^{3+} lifetime in these materials, thermal gratings were not observed. Additionally, as the wavelength dependence of the FWM signal did not correlate with the excited-state absorption spectrum of GSGG:Cr^{3+}, absorptive contributions were not observed. Finally, the results were analyzed using the formula derived for a phase grating and the predicted intensity and lifetime dependences were confirmed.

In the discussion, we provided explanations for the origin of the refractive index change due to the excited-state population. The large oscillator strength of the charge-transfer transitions in the energy region of 50 000 cm^{-1} in oxides were seen to account for the polarizability change observed. The strongest absorptions observed in this energy region for the fluoride host crystals, however, were the interconfigurational $3d\rightarrow 4s$ type which are characterized by much weaker oscillator strengths, thus accounting for our observation that the fluoride hosts did not give measurable signal levels.

In the oxide crystals studied, the polarizability change was observed to depend on the relative thermal population of the $^4T_2$ and ^2E excited levels, and our fit to the data gave a $^4T_2$ state polarizability change of 0.155 Å^3, while the ^2E value was 0.017 Å^3. Lastly, we found that

the $ScBO_3$ host behaved differently than the other materials due to the strong complexation of oxygen in the borate groups.

ACKNOWLEDGMENTS

This research was performed under the auspices of the Division of Materials Sciences of the Office of Basic Energy Sciences, U.S. Department of Energy, and the Lawrence Livermore National Laboratory under Contract No. W-7405-ENG-48. This research was also supported by the DOE under research Grant No. DE-FG02-84ER45146, and we are especially indebted to Professor D. S. McClure of Princeton University for making this financial support available to us. We wish to thank Gary Wilke for assembling the optics and laser system used in this experiment, Dr. L. L. Chase for many helpful discussions and especially for suggesting that we carefully examine the role of the charge-transfer bands, and Robert Adair for generously sharing his experimental and scientific expertise with us. We wish to thank B. Chai of Allied Signal Corp. for the $ScBO_3$, $La_3Ga_5SiO_{14}$, and $BeAl_2O_4$ samples, H. Guggenheim of A.T.T. Bell Laboratories (retired) for the $Na_3Ga_2Li_3F_{12}$ and $SrAlF_5$ samples, H. Newkirk for the Ga_2O_3, $LiCaAlF_6$, and $LaMgAl_{11}O_{19}$ samples, and E. Prochnow for polishing these samples.

[1]M. B. Klein and R. N. Schwartz, J. Opt. Soc. Am. B **3**, 293 (1986).
[2]C. M. Lawson, R. C. Powell, and W. K. Zwicker, Phys. Rev. B **26**, 4836 (1982).
[3]J. K. Tyminski, R. C. Powell, and W. K. Zwicker, Phys. Rev. B **29**, 6074 (1984).
[4]R. C. Powell, J. K. Tyminski, A. M. Ghazzawi, and C. M. Lawson, IEEE J. Quantum Electron. **QE-22**, 1355 (1986).
[5]G. P. Morgan, S. Chen, and W. M. Yen, IEEE J. Quantum Electron. **QE-22**, 1360 (1986).
[6]R. W. Boyd, M. T. Gruneisen, P. Narum, D. J. Simkin, B. Dunn, and D. L. Yang, Opt. Lett. **11**, 162 (1986).
[7]S. C. Rand, J. F. Lam, R. S. Turley, R. A. McFarlane, and O. M. Stafsudd, Phys. Rev. Lett. **59**, 597 (1987).
[8]F. M. Durville, E. G. Behrens, and R. C. Powell, Phys. Rev. B **34**, 4213 (1986).
[9]F. M. Durville, E. G. Behrens, and R. C. Powell, Phys. Rev. B **35**, 4109 (1987).
[10]F. M. Durville and R. C. Powell, J. Opt. Soc. Am. B **4**, 1934 (1986).
[11]A. Suchocki, J. D. Allen, R. C. Powell, and G. M. Loiacono, Phys. Rev. B **36**, 6729 (1987).
[12]P. F. Liao and D. M. Bloom, Opt. Lett. **3**, 4 (1978).
[13]D. S. Hamilton, D. Heiman, J. Feinberg, and R. W. Hellwarth, Opt. Lett. **4**, 124 (1979).
[14]P. F. Liao, L. M. Humphrey, D. M. Bloom, and S. Geschwind, Phys. Rev. B **20**, 4145 (1979).
[15]S. A. Boothroyd and C. G. Morgan, J. Phys. D **16**, L165 (1983).
[16]H. I. Mandelberg, Opt. Lett. **5**, 258 (1980).
[17]A. M. Ghazzawi, J. K. Tyminiski, R. C. Powell, and J. C. Walling, Phys. Rev. B **30**, 7182 (1984).
[18]A. Suchocki, G. D. Gilliland, and R. C. Powell, Phys. Rev. B **35**, 5830 (1987).
[19]G. D. Gilliland, A. Suchocki, K. W. Ver Steeg, R. C. Powell, and D. F. Heller, Phys. Rev. B **38**, 6227 (1988).
[20]D. G. Steel and S. C. Rand, Phys. Rev. Lett. **55**, 2285 (1985).
[21]D. G. Steel, S. C. Rand, and J. Liu, J. Opt. Soc. Am. B **4**, 1794 (1987).
[22]T. Catunda, J. P. Andreeta, and J. C. Castro, Appl. Opt. **25**, 2391 (1986).
[23]T. Catunda and J. C. Castro, Opt. Commun. **63**, 185 (1987).
[24]A. Suchocki and R. C. Powell, Chem. Phys. (to be published).
[25]G. J. Quarles, A. Suchocki, R. C. Powell, and S. Lai, Phys. Rev. B **38**, 9996 (1988).
[26]F. M. Durville, R. C. Powell, G. Boulon, and B. Champagnon, Phys. Rev. B **37**, 1435 (1988).
[27]H. Eichler, P. Glozbach, and B. Kluzowski, Z. Angew. Phys. **28**, 303 (1970).
[28]K. O. Hill, Appl. Opt. **10**, 1695 (1971).
[29]H. Kogelnik, Bell Syst. Tech. J. **48**, 2909 (1969).
[30]H. Eichler, G. Salje, and H. Stahl, J. Appl. Phys. **44**, 5383 (1973).
[31]H. J. Eichler, J. Eichler, J. Knof, and Ch. Noack, Phys. Status Solidi A **52**, 481 (1979).
[32]R. L. Abrams and R. C. Lind, Opt. Lett. **2**, 94 (1978).
[33]The optical values used for $GdAlO_3$: $n=2.0$, $\tau=10$ ms, $\sigma_g=2.5\times10^{-20}$ cm^2 (at the peak of the $^4T_2$ band), and the peak emission wavelength, $\lambda=730$ nm, were obtained from Refs. 21, 22, and 23. The thermal values used: $\kappa=0.1097$ W/K cm and $dn/dT=9.7\times10^{-6}$ K^{-1}, are for the structurally similar $YAlO_3$ and were obtained from *Handbook of Laser Science and Technology,* edited by M. J. Weber (CRC, Boca Raton, 1986), Vol. 5, Part 3, Sec. 1.5.
[34]R. G. Caro and M. C. Gower, IEEE J. Quantum Electron. **QE-18**, 1376 (1982).
[35]*Nonlinear Optics of Free Atoms and Molecules,* Vol. 17 of *Springer Series in Optical Sciences,* edited by D. C. Hanna, M. A. Yuratich, and D. Cotter (Springer-Verlag, New York, 1979).
[36]A. Yariv and R. A. Fisher, in *Optical Phase Conjugation,* edited by R. A. Fisher (Academic, New York, 1983), pp. 7–10, 41, and 42.
[37]A. Yariv, *Quantum Electronics,* 2nd ed. (Wiley, New York, 1975), Chap. 8.
[38]G. Martin and R. W. Hellwarth, Appl. Phys. Lett. **34**, 371 (1979).
[39]H. Eichler, G. Enterlein, J. Munschau, and H. Stahl, Z. Angew. Phys. **31**, 1 (1970).
[40]W. L. Smith, in *Handbook of Laser Science and Technology,* edited by M. J. Weber (CRC, Boca Raton, 1986), Vol. 3, Part 1.
[41]R. C. Powell, L. Xi, X. Gang, G. J. Quarles, and J. C. Walling, Phys. Rev. B **32**, 2788 (1985).
[42]K. L. Schepler, J. Appl. Phys. **56**, 1314 (1984).
[43]A. P. Eliseev, A. M. Yurkin, and E. G. Samoilova, Phys. Status Solidi A **105**, K169 (1988).
[44]M. D. Shinn, W. F. Krupke, J. A. Caird, and H. W. Newkirk, in *Advances in Laser Science—1 (University of Texas, Dallas, Texas, 1985),* Proceedings of the First International Laser Science Conference, AIP Conf. Proc. No. 146, edited by W. C. Stwalley and M. Lapp (AIP, New York, 1985).
[45]A. Siegman, *Lasers* (University Science Books, Mill Valley, 1986), Chap. 6.

[46]Our difference spectra agrees well with the published data: L. J. Andrews, S. M. Hitelman, M. Kokta, and D. Gabbe, J. Chem. Phys. **84**, 5229 (1986).
[47]J. A. Caird, S. A. Payne, P. R. Staver, A. J. Ramponi, L. L. Chase, and W. F. Krupke, IEEE J. Quantum Electron. **QE-24**, 1077 (1988).
[48]W. F. Krupke, M. D. Shinn, J. E. Marion, J. A. Caird, and S. E. Stokowski, J. Opt. Soc. Am. B **3**, 102 (1986).
[49]J. V. Meier, N. P. Barnes, D. K. Remelius, and M. R. Kokta, IEEE J. Quantum Electron. **QE-22**, 2058 (1986).
[50]A. Biedl, Am. Mineral. **51**, 521 (1966).
[51]J. C. Walling, O. G. Peterson, H. P. Jenssen, R. C. Morris, and E. W. O'Dell, IEEE J. Quantum Electron. **QE-16**, 1302 (1980).
[52]M. J. Dodge, in *Handbook of Laser Science and Technology,* edited by M. J. Weber (CRC, Boca Raton, 1986), Vol. 4, Part 2, Sec. 1.1.1.2.
[53]Kh. S. Bagdasarov, L. M. Dorozhkin, L. A. Ermakova, A. M. Kevorkov, Y. I. Krasilov, N. T. Kuznetsov, I. I. Kuratev, A. V. Potemkin, L. N. Raiskaya, P. A. Tseitlin, and A. V. Shestakov, Kvant. Elektron. (Moscow) **10**, 1645 (1983) [Sov. J. Quantum Electron. **13**, 1082 (1983)].
[54]The refractive index for $La_3Ga_5SiO_{14}:Cr^{3+}$ was estimated from the indices of the constituent oxide compounds.
[55]A. A. Kaminskii, A. P. Shkadarevich, B. V. Mill', V. G. Koptev, and A. A. Demidovich, Izv. Akad. Nauk SSSR Neorg. Mater. **23**, 690 (1987) [Inorg. Mater. (USSR) **23**, 618 (1987)].
[56]S. A. Payne, L. L. Chase, H. W. Newkirk, L. K. Smith, and W. F. Krupke, IEEE J. Quantum Electron. **24**, 2243 (1988).
[57]V. I. Vasil'tsiv and Ya. M. Zakarko, Zh. Prikl. Spektrosk. **39**, 423 (1983) [J. Appl. Spectrosc. (USSR) **39**, 1037 (1983)].
[58]S. T. Lai, B. H. T. Chai, M. Long, and R. C. Morris, IEEE J. Quantum Electron. **QE-22**, 1931 (1986).
[59]F. Michel-Calendini, H. Chermette, and G. Boulon, J. Lumin. **40&41**, 309 (1988).
[60]H. P. Jenssen and S. T. Lai, J. Opt. Soc. Am. B **3**, 115 (1986).
[61]S. A. Payne, L. L. Chase, and G. D. Wilke, J. Lumin. (to be published).
[62]B. Struve and G. Huber, Appl. Phys. B **36**, 195 (1985).
[63]R. C. Powell, A. Sushocki, G. D. Gilliland, and G. J. Quarles, J. Lumin. **38**, 250 (1987).
[64]D. Vivien, B. Viana, A. Revcolevschi, J. D. Barrie, B. Dunn, P. Nelson, and O. M. Stafsudd, J. Lumin. **39**, 29 (1987).
[65]H. H. Tippins, Phys. Rev. B **1**, 126 (1970).
[66]T. Kushida, J. Phys. Soc. Jpn. **21**, 1331 (1966).
[67]W. Kauzmann, *Quantum Chemistry* (Academic, New York, 1957), Chap. 15.
[68]J. F. Sabatini, A. E. Salwin, and D. S. McClure, Phys. Rev. B **11**, 3832 (1975).
[69]J. R. Tessman, A. H. Kahn, and W. Shockley, Phys. Rev. **92**, 890 (1953).
[70]*Handbook of Chemistry and Physics,* 68th ed., edited by R. C. Weast (CRC, Boca Raton, 1987), Sec. B.
[71]J. Shanker, G. G. Agrawal, and N. Dutt, Phys. Status Solidi B **138**, 9 (1986).
[72]W. M. Yen, L. R. Elias, and D. L. Huber, Phys. Rev. Lett. **24**, 1011 (1970).